Clean Energy, 2022, Vol. 6, No. 5, 762–775
https://doi.org/10.1093/ce/zkac057
Advance access publication 28 October 2022
Research Article

Maximum power point tracking using decision-tree machine-learning algorithm for photovoltaic systems

P. Venkata Mahesh[1,3,*], S. Meyyappan[1,2] and RamaKoteswara Rao Alla[3]

[1]Department of Electronics and Instrumentation Engineering, Annamalai University, Chidambaram, India
[2]Department of Instrumentation Engineering, Madras Institute of Technology, Chennai, India
[3]Department of EEE, RVR & JC College of Engineering, Guntur, India
*Corresponding author. E-mail: vnktmahesh@gmail.com

Abstract

This work presents a machine-learning (ML) algorithm for maximum power point tracking (MPPT) of an isolated photovoltaic (PV) system. Due to the dynamic nature of weather conditions, the energy generation of PV systems is non-linear. Since there is no specific method for effectively dealing with the non-linear data, the use of ML methods to operate the PV system at its maximum power point (MPP) is desirable. A strategy based on the decision-tree (DT) regression ML algorithm is proposed in this work to determine the MPP of a PV system. The data were gleaned from the technical specifications of the PV module and were used to train and test the DT. These algorithms predict the maximum power available and the associated voltage of the module for a defined amount of irradiance and temperature. The boost converter duty cycle was determined using predicted values. The simulation was carried out for a 10-W solar panel with a short-circuit current of 0.62 A and an open-circuit voltage of 21.50 V at 1000 W/m^2 irradiance and a temperature of 25°C. The simulation findings demonstrate that the proposed method compelled the PV panel to work at the MPP predicted by DTs compared to the existing topologies such as β-MPPT, cuckoo search and artificial neural network results. From the proposed algorithm, efficiency has been improved by >93.93% in the steady state despite erratic irradiance and temperatures.

Graphical Abstract

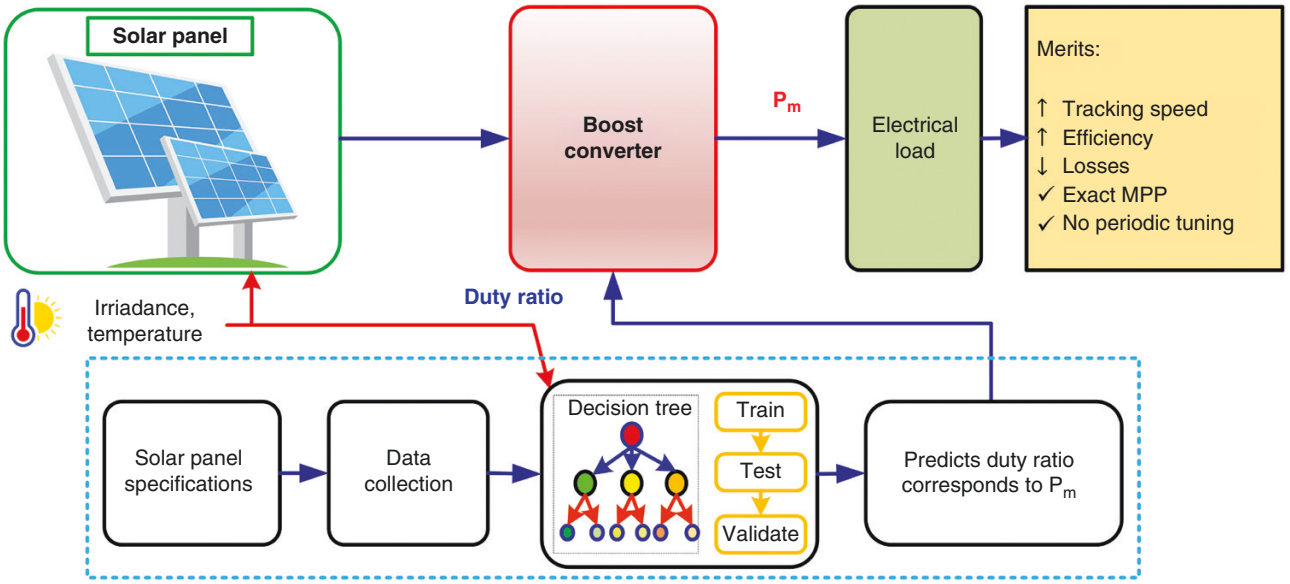

Keywords: boost converter; decision tree; maximum power point tracking; photovoltaic system; regression machine learning

Introduction

Every nation must have access to inexpensive, sustainable electricity to advance industrially, socially and economically. Due to industrialization and urbanization, India's energy needs are continually increasing. India, a developing nation, added a total installed electricity capacity from various sources from 1.362 GW in 1947 to 403.7 GW as of 30 June 2022 [1, 2]. Clearly, since

Received: 1 July 2022. **Accepted:** 16 September 2022

the country's independence, coal and lignite have been India's primary sources of power supply. However, due to the massive emissions of heavy metals and polluting chemicals from the stack of these traditional power generators, humans are harmed by them.

Fig. 1 illustrates the sources of installed electrical energy in India as a percentage. As of 30 June 2022, India's total installed generating capacity was 403.76 GW, with thermal accounting for 58.47%, renewable accounting for 28.25%, nuclear accounting for 1.68% and hydro accounting for 11.6% [2, 3]. Coal-based power accounted for 52.18% of the energy supply in the Indian electrical grid. The hybridization of diverse renewable energy sources with energy-storage technologies, which play a vital role in addressing power uncertainties, may minimize dependence on traditional energy sources. In the current context, any country's power distribution system regards energy storage as a critical component. This is because preserving fossil fuels may improve grid stability, boost system efficiency, promote renewable-energy penetration and assist in alleviating environmental and health effects. Adopting battery energy-storage system technology can also minimize the operational costs of the power distribution network. Thus, combining solar energy with energy-storage technology improves rural energy availability, boosting economic growth [4].

Renewable energy will provide a sustainable alternative as a green and pollution-free power source to meet India's electricity needs [4]. Table 1 shows that the total installed capacity of renewable energy from various sources was 114.065 GW as of 30 June 2022 [3]. As a result of the above facts, solar power has emerged as a critical source of green power among renewable energy, making

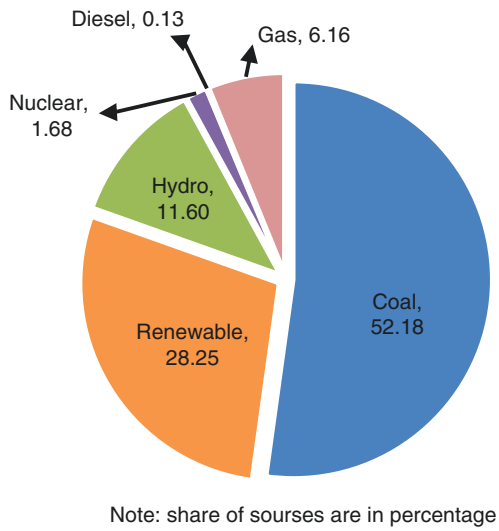

Fig. 1: Installed capacity of electricity in India by source.Source: Central Electricity Authority, India. Note: shares of sources are in percentages.

Table 1: Renewable-energy installed capacity

Renewable energy sources	Installation capacity (MW)	Share (%)
Wind	40 788	35.76
Solar	57 706	50.59
Biomass	10 206	8.95
Waste to energy	477	0.42
Small hydro	4888	4.29
Total	114 065	100.00

history for the country's growth and reaching new heights in the Indian power industry.

The sun is the most easily available energy source on Earth among all renewable energy sources. Solar energy is converted into electrical energy using photovoltaic (PV) cells. The PV panel should run at its MPP, or the greatest power possible, to generate as much energy as possible under the specified operating parameters. A maximum power point tracking (MPPT) method is required since the MPP varies with the temperature and solar radiation of the environment. An MPPT algorithm should ideally enhance PV panel output power independently of solar irradiation, ambient temperature and shifting weather conditions. As a result, both the amount of energy created and the efficiency of the power generation are improved. Popular MPPT techniques in the literature include conventional methods such as perturb and observe (P&O) [5] and incremental conductance [6, 7], which use the panel current and voltage for tracking the MPP. Mathematical-based methods such as β-MPPT [8] and curve fitting [9] use calculations related to the various equations to identify the MPP. Constant parameter methods include fractional open-circuit voltage [10] and short-circuit current [11], which require periodic open-circuit and short-circuit current of the load, respectively. Optimization MPPT methods such as cuckoo search (CS) [12], particle swarm optimization (PSO) [12, 13], ant colony optimization [14] and genetic algorithm [14, 15] methods will try to optimize (either maximize or minimize) a function. Intellectual prediction methods include the artificial neural network [16–19] method that requires the data set to train the model and the fuzzy-logic control method [20–23] that needs prior knowledge of the data to create a strong rule base. The merits and demerits of various MPPT methods are tabulated in Table 2.

Machine-learning algorithms (MLAs) are best suited to handle non-linear PV data. The accuracy and speed of the MPP's tracking can be increased by employing MLA. Reinforcement learning [29], image-based machine learning (ML) [30] and the random forest method [31] are applied to track the MPP of PV systems in the literature. MLA will predict the anonymous data if it goes through training, testing and validation using existing data. In general, 60% of the data are used for training, 20% for testing and the remaining data are used to validate the ML model. In the following Equations (1) and (2), root mean square error (RMSE) and R^2 values represent the model's performance:

$$RMSE = \sqrt{\frac{1}{n_s}\sum_{k=1}^{n_s}\left(y_{t,k} - y_{p,k}\right)^2} \quad (1)$$

$$R^2 = 1 - \frac{\sum_{k=1}^{n_s}\left(y_{t,k} - y_{p,k}\right)^2}{\sum_{k=1}^{n_s}\left(y_{t,k} - y_{ag}\right)^2} \quad (2)$$

where the true value is y_t, the predicted value is y_p, the total count of samples is n_s and the true values average is y_{ag}. The R^2 value is in between zero and 1, which provides the prediction strength of the model and for the best-fitted model, the R^2 value is close to 1. Similarly, the *RMSE* values are measures of the error between y_p and y_t. Therefore, the value of the *RMSE* that is close to zero represents the model with greater strength of prediction.

This research article is organized as follows. Section 1 describes the system, which includes the specifications and characteristics of the PV panel, the boost converter and the regression-tree (RT) algorithm. Section 2 describes the methodology for data collection, model preparation and the MPPT RT control approach to the solar panel. Section 3 provides the results of the simulation and discussions. Finally, Section 4 of the study provides a comparative evaluation of the different MPPT

control mechanisms provided in the literature with the proposed method, along with a conclusion in Section 5.

1 System description

1.1 PV panel, characteristics and mathematical model

A PV cell converts solar energy into DC electrical energy through a physical process called the photoelectric effect. A PV array is a collection of PV cells connected in parallel and in series to increase the voltage and current within the array. Fig. 2 depicts a more accurate circuit model of a solar PV cell. Series resistance (R_s) and shunt resistances (R_{sh}) are ideally neglected but, in practice, this is not practical because these factors impact the efficiency of the PV solar cell. From Fig. 2, the output current I is as follows:

$$I = I_{PH} - I_D - I_{sh} \tag{3}$$

where I_{PH} is the light-produced current, I_D is diode current and I_{sh} is the current through R_{sh}. R_s in the current path is a loss caused by the Joule effect and is primarily caused by metal grids, semiconductor materials, the collecting bus and its connections. R_{sh} stands for shunt resistances and is connected with current seepage owing to cell thickness and surface effects. Compared to R_{sh}, the impact of R_s is more pronounced due to the expansion of the cell resistance in the PV module. The influence of R_{sh} is only seen when there are a high number of PV modules in the solar PV system. So, if R_s is taken into account and R_{sh} is assumed to be infinite, then the diode current is represented in Equation (4):

$$I_D = I_0\left(e^{\frac{q(V+IR_s)}{N_s nKT}} - 1\right) \tag{4}$$

where q is the electron charge, K is Boltzmann's constant, cell temperature is T and the diode ideal factor is n ($1 \le n \le 2$). The output current I is given by Equation (5):

$$I = I_{PH} - I_0\left(e^{\frac{q(V+IR_s)}{N_s nKT}} - 1\right) - \frac{V + IR_s}{R_{sh}} \tag{5}$$

When the PV cells are connected in series–parallel and the output current I is determined, Equation (5) may be changed and is shown in Equation (6) as follows:

$$I = N_p \times I_{PH} - N_p \times I_0\left(e^{\frac{q(V+IR_s)}{N_s nKT}} - 1\right) - \frac{N_p}{R_s}\left(\frac{V}{N_s} + \frac{R_s\, I}{R_p}\right) \tag{6}$$

where N_p and N_s indicate the number of parallel and series connected cells, respectively. According to the I_{PH} equation given in Equation (7), the photocurrent is proportional to the incoming flux and independent of V (or R_s); it is linearly dependent on solar radiation (G) and is also impacted by temperature [4]. The reference solar radiation (G_{ref}) is 1000 W/m^2:

$$I_{PH} = [I_{sc} + K_i\,(T - T_r)] \times \frac{G}{G_{ref}} \tag{7}$$

where $K_i = \frac{I_{sc(To)} - I_{sc(Tref)}}{T_o - T_r}$.

I_{sc} is the short-circuit current, and T and T_r (25°C) are real-time and reference temperatures, respectively. Equations (8) and (9) are used to compute the reverse saturation current (I_{rs}) and the saturation current (I_o):

$$I_{rs} = I_{sc}/\left(e^{\frac{q\ V_{oc}}{N_s nKT}} - 1\right) \tag{8}$$

$$I_o = I_{rs}\left[\frac{T}{T_r}\right]^3 e^{\left[\left(\frac{q\ Eg}{nk}\right)\left(\frac{1}{T_r} - \frac{1}{T}\right)\right]} \tag{9}$$

Table 2: Analysis of MPPT methods with limitations

Reference	MPPT algorithm	Contributions	Limitations	Year
M. Shixun *et al.* [24]	Mayfly intelligent optimization	Studied under uniform and non-uniform illuminations. Can track MPP by two populations	Compared with only the PSO algorithm. Temperature fixed at 25°C	2022
S.R. Revathy *et al.* [25]	Adaptive neuro-fuzzy inference system	PV array of five Canadian Solar CS5C-80M modules serially connected to a boost converter. 231 data sets acquired from the I–V and P–V characteristics	Limited shading patterns considered. Complex rule base and system with five layers	2022
K.R. Ahmed *et al.* [26]	Deep learning	Deep learning with back propagation neural network is employed. A two-stage control is employed	Just the methodology is stated not simulated	2022
H. Islam *et al.* [27]	Proportional integral (PI) control	Results in fast-tracking and reduced power oscillations. The PV system is connected to the grid through an H-bridge inverter	Effect of temperature is not considered. Proper tuning is required for PI controller	2021
R.M. Asif *et al.* [20]	Modified fuzzy-logic algorithm	MPPT power loss reduction. Consider severe climatic drifts. Charging management control is implemented on the lead-acid battery bank to store photovoltaic energy for backup use. To maintain the state of charge (SOC) of the batteries, the charging and discharging time are calculated using a C-rate scale	The effect of temperature on battery charging/discharging is not considered. The lifetime of the battery is not considered	2021
K. Rajani, T. Ramesh [28]	Sudoku reconfiguration technique	MPPT under partial shading condition. Performance analysis carried out in terms of global maximum power (GMP), fill factor, mismatch losses and efficiency	Wiring complexity increases	2020
S. Dorji *et al.* [6]	P&O and fuzzy logic control (FLC)	For boost converter and quadratic boost converter is carried and compared	Simulated under only standard test conditions. Dynamic weather conditions not considered	2020
X. Li *et al.* [22]	β parameter-based FLC	A novel β-parameter-based FLC is coined with three inputs and one output, and this β method will reduce the number of membership functions	The temperature effect is not considered. The sensitivity of V and I sensing devices are not taken into account	2019

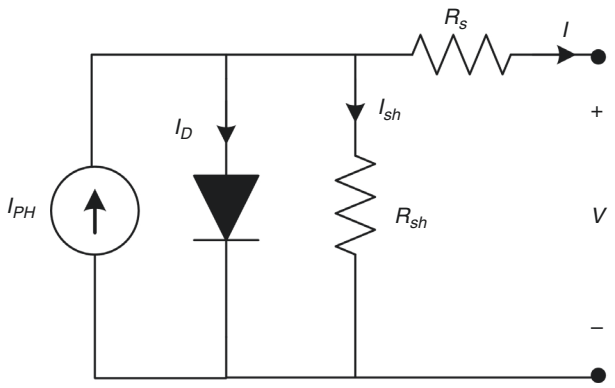

Fig. 2: The one-diode equivalent circuit of a PV cell.

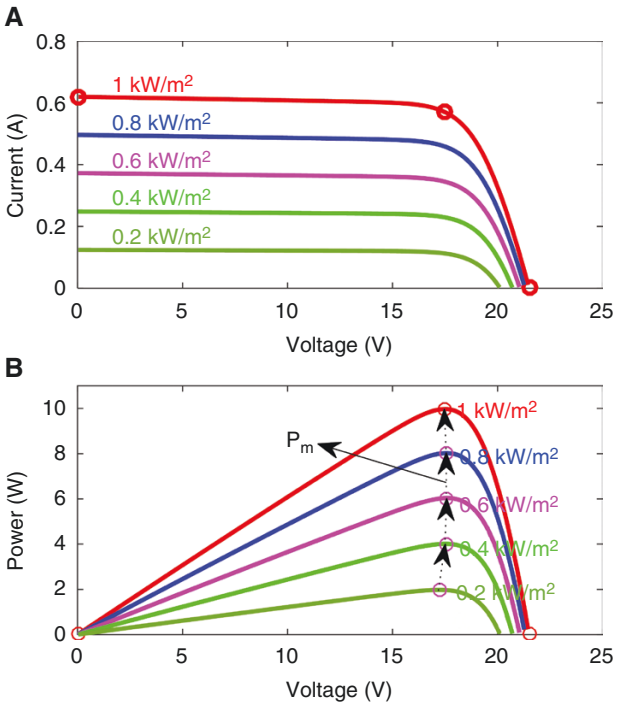

Fig. 3: Characteristics of PV panel with provided irradiances at 25°C.(a) V vs I; (b) V vs P.

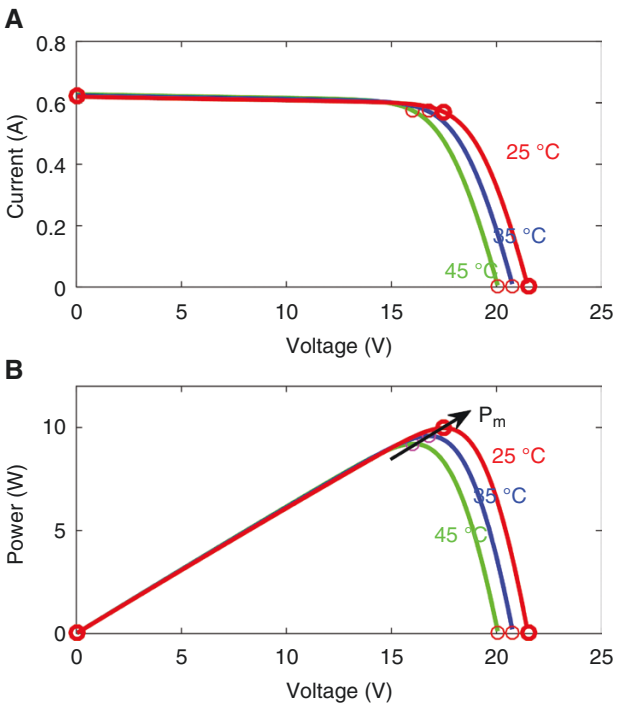

Fig. 4: Characteristics of PV panel with provided temperatures at 1000 W/m².(a) V vs I; b) V vs P.

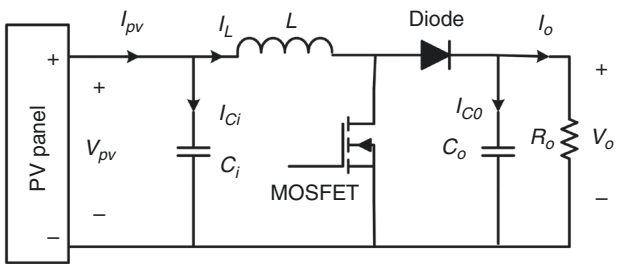

Fig. 5: The PV supplied boost converter circuit.

In this work, a PV panel whose specifications are a maximum power capacity of 10 W with a short-circuit current of 0.62 A and an open-circuit voltage of 21.50 V, the voltage and current at MPP are 17.50 V and 0.57 A, respectively, and with 36 solar cells used for simulation. Figs 3 and 4 show the I–V and P–V characteristics of the panel for a range of temperatures and irradiances.

1.2 DC–DC boost converter

Fig. 5 shows a DC–DC boost converter powered by a PV panel and controlled by pulse width modulation (PWM). The metal oxide field effect transistor duty ratio (D) influences the power transferred from the panel to the load. The circuit increases the PV voltage to the expected output level by an inductor (L). The input capacitor (C_i) and output capacitor (C_o) minimize the ripple content of the output voltages. The boost inductor's current grows linearly while the switch is in the on position and the diode is off. The inductor's stored energy is released when the switch is off, passing via the diode and onto the output R_oC_o circuit. The capacitive filter smoothes the switching action's pulsing current while supplying a DC voltage to the load.

2 DT ML algorithm

A DT is a ML algorithm generally used for regression and classification problems. The output of a classification-type tree is a class or label of the data, whereas the RT output is a real value. A RT is a DT meant to approximate real-valued functions rather than be utilized for categorization. The input variables may include both continuous and categorical data when using the standard RT building method. The tree is referred to as a DT when each decision node tests the value of an input variable. The terminal nodes of the tree contain the predicted output variable values. Binary recursive partitioning is an iterative approach that splits data into branches or partitions and divides each branch into smaller units as the procedure continues along each partition. The training set's records (pre-classified data used to define the tree's architecture) are first sorted into the same division. The approach then separates the data into two segments or branches, using each field's possible binary split.

The method chooses a division that reduces the sum of squares of the deviations from the mean of the two independent divisions. Then this rule is used to split each new branch. This operation

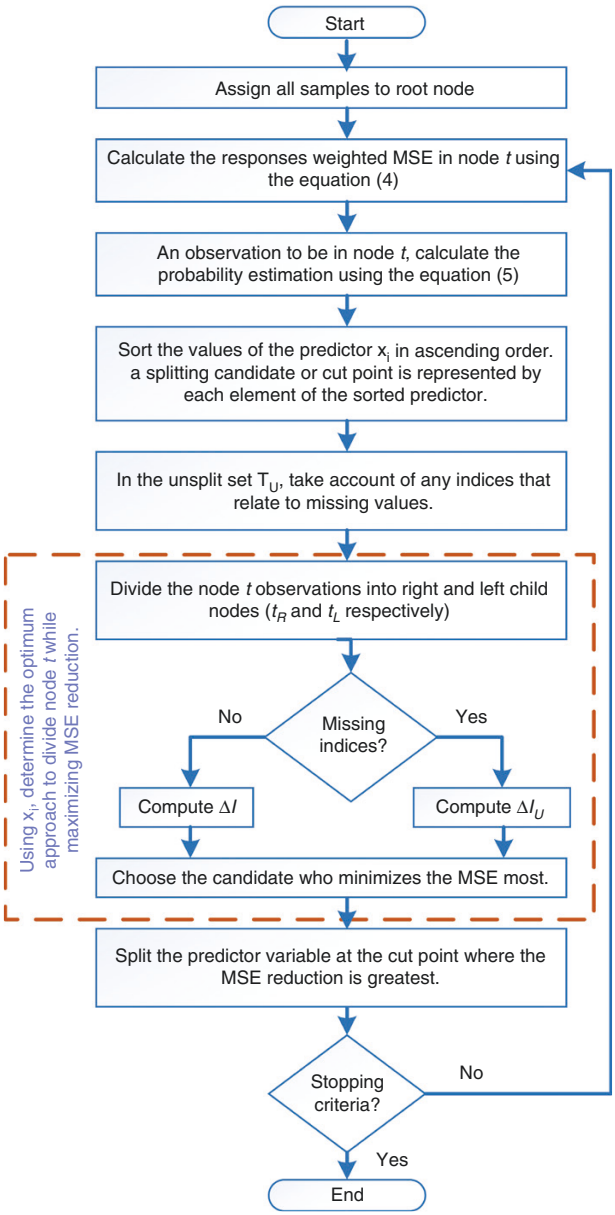

Fig. 6: Flowchart of node-splitting procedure for CART.

continues until each node reaches the user-specified minimum node size and becomes a terminal node. Even if a node does not meet the minimum size requirement, if its sum of squared deviations from the mean is zero, it is considered a terminal node. The stepwise procedure for standard classification and regression tree (CART) with all predictors x_i ($i = 1,2,\ldots, p$) to split node t is shown in Fig. 6. The basic structure of a DT is shown in Fig. 7.

The weighted mean squared error (MSE) of the response in node t is given by Equation (10):

$$\varepsilon_t = \sum_{j \in T_t} w_j \, (y_j - \bar{y}_t)^2 \tag{10}$$

where w_j is j^{th} observation weight and the set of all observation indices in node t is denoted by T_t. If no weights are specified, use $w_j = 1/n$ and n as the sample size. Probability estimation is given by Equation (11):

$$P(T_t) = \sum_{j \in T_t} w_j \tag{11}$$

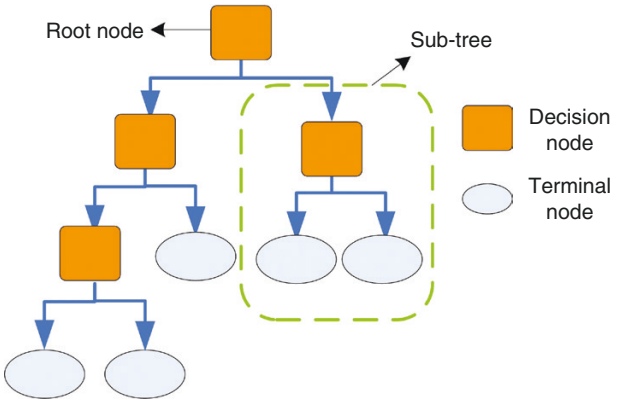

Fig. 7: Illustration of the RT problem.

For $t_L \in T_L$ and $t_R \in T_R$, the decrease in MSE for the present splitting data point is (if x_i does not have any missing values) given by Equation (12):

$$\Delta I = P(T_t)\,\varepsilon_t - P(T_L)\,\varepsilon_{tL} - P(T_R)\,\varepsilon_{tR} \tag{12}$$

The reduction in MSE is (if x_i has missing values, with an assumption that there are randomly missing observations) given by Equation (13):

$$\Delta I_U = P(T_t - T_U)\,\varepsilon_t - P(T_L)\,\varepsilon_{tL} - P(T_R)\,\varepsilon_{tR} \tag{13}$$

where $T_t - T_U$ is the collection of all valid observation indices for node t.

3 Methodology

The proposed approach consists of two steps and involves building the RT ML model using the data obtained based on the PV panel parameters and using the prepared model for MPPT. First, since irradiance (I_r) and T are functions of the maximum power (P_m) and the respective voltage (V_m) at MPP, I_r and T are used as features to predict the data for P_m and V_m. Therefore, the created models are utilized for the specified I_r and T to predict the PV panel's P_m and V_m. Then, the predicted values are used to determine the duty cycle (D) to drive the PV panel at MPP.

3.1 Data collection and model preparation

I_r, T, P and V make up the data needed to train and test the model. Fig. 8 shows a flowchart of the conceptual process of collecting data and creating a ML model.

3.2 MPPT with boost converter and RT model

The prepared ML model predicts the available maximum power in the PV panel (P_m) and the respective voltage (V_m) for the features I_r and T. Using the predicted values P_m, V_m as in Equation (14), the resistance R_{mp} that corresponds to MPP is computed. By adjusting the D of the converter, the R_{mp} will be reproduced between node-n_1 and node-n_2 in Fig. 9. In Equation (15), the load resistance (R_0) and R_{mp} provide the converter's D:

$$R_{mp} = \frac{V_m^2}{P_m} \tag{14}$$

$$D = 1 - \sqrt{\frac{R_{mp}}{R_0}} \tag{15}$$

The approach suggested by Ayop *et al.* [32] can be used to estimate the highest and lowest values of the resistance for the load. The process outlined by Rashid [33] was used to design

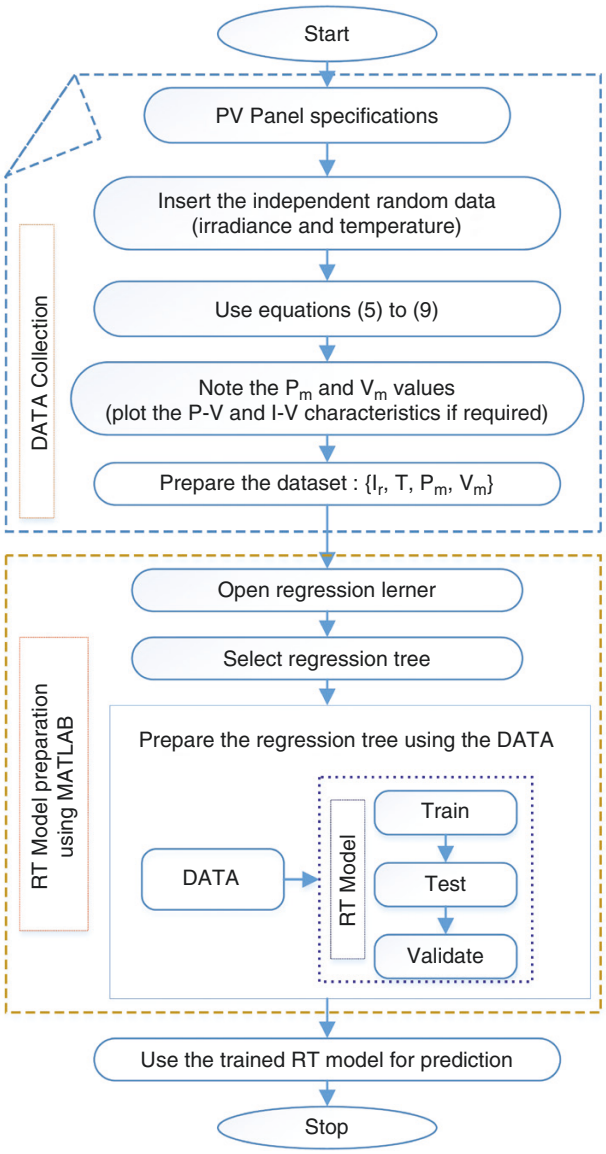

Fig. 8: Flowchart of the schematic procedure for data collection and ML model preparation.

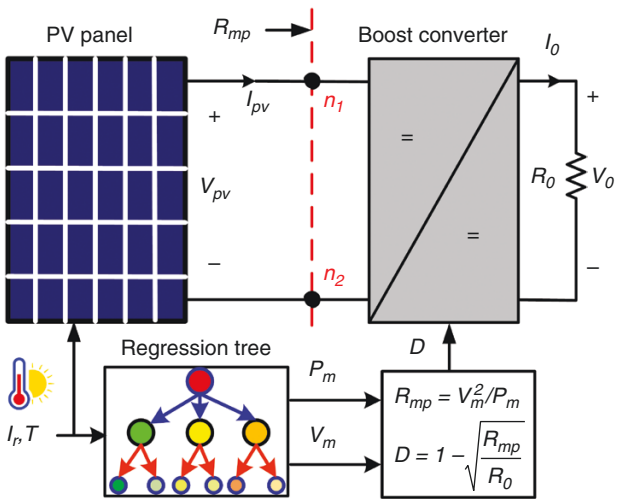

Fig. 9: Schematic of the solar panel with the RT ML control method and DC–DC boost converter.

the boost converter. The inductance for a boost converter is given by Equation (16), while the capacitance is given by Equation (17):

$$L = \frac{V_{ip} \times (V_{op} - V_{ip})}{f_{sw} \times \Delta I \times V_{op}} \tag{16}$$

$$C = \frac{I_{op} \times (V_{op} - V_{ip})}{f_{sw} \times \Delta V \times V_{op}} \tag{17}$$

where f_{sw} is the switching frequency in hertz, ΔI stands for the percentage current ripple, ΔV for the percentage voltage ripple, and V_{ip} and V_{op} are the input and output voltages in volts, respectively. Fig. 9 shows the block diagram of the PV panel associated with the RT ML control technique of the RT and the boost converter.

4 Simulation results and discussion

With the use of PV panel parameters, the data for PV panels have been gathered in the proposed approach, as mentioned in Section 3. The pairwise association between the data is shown in Fig. 10. In Fig. 11, a correlation heat map visually and numerically represents the relationship between the variables.

The simulation was run at four intervals of 0.5 sec each for a total of 2 sec to determine the tracking accuracy of the RT under various irradiances and temperatures. For each interval, the values of I_r or T are changed while keeping the other fixed. Table 3 displays this change.

The parameters for simulation are:

- rated PV power = 10 W;
- voltage ripple, ΔV = 1%;
- current ripple, ΔI = 5%;
- designed boost converter:
  - switching frequency, f_{sw} = 5 kHz;
  - inductance, L = 34 mH;
  - capacitance, C_o = 68 μF;
- load resistance = 300 Ω;
- input capacitance, C_i = 1000 μF.

I_r and T are used as the input to create two RTs, P_m and V_m being the predicted responses for each. Figs 12 and 13 show the trained RTs on P_m and V_m planes using MATLAB® software. Fig. 14 shows the actual data as well as the expected data from the created RT models. Since the RT technique performs an averaging function on the data, the residual in prediction will be modest if the actual values are near the average values and will be as high as possible up to the maximum. Fig. 15 displays the estimations of predictor importance. The x-axis represents each model predictor and the y-axis measures their significance. This significance has no unit and is defined as the sum of their MSE when permutation in the RTs is done. The predictors x_1 and x_2 are I_r and T, respectively.

Table 3 shows the RT model's predicted P_m and V_m values, the computed duty cycle and the mean efficiency in steady state. The V, I and P waveforms of the solar panel and load are shown in Fig. 16, employing RT models. These findings indicate that when the T is changed, there are moderate oscillations in the transient response and significant amplitude oscillations when the I_r is altered. Finally, the mean efficiency is shown in Fig. 17, along with a comparison between predicted power and PV operational power. It shows that the suggested approach correctly tracks the MPP in the steady state.

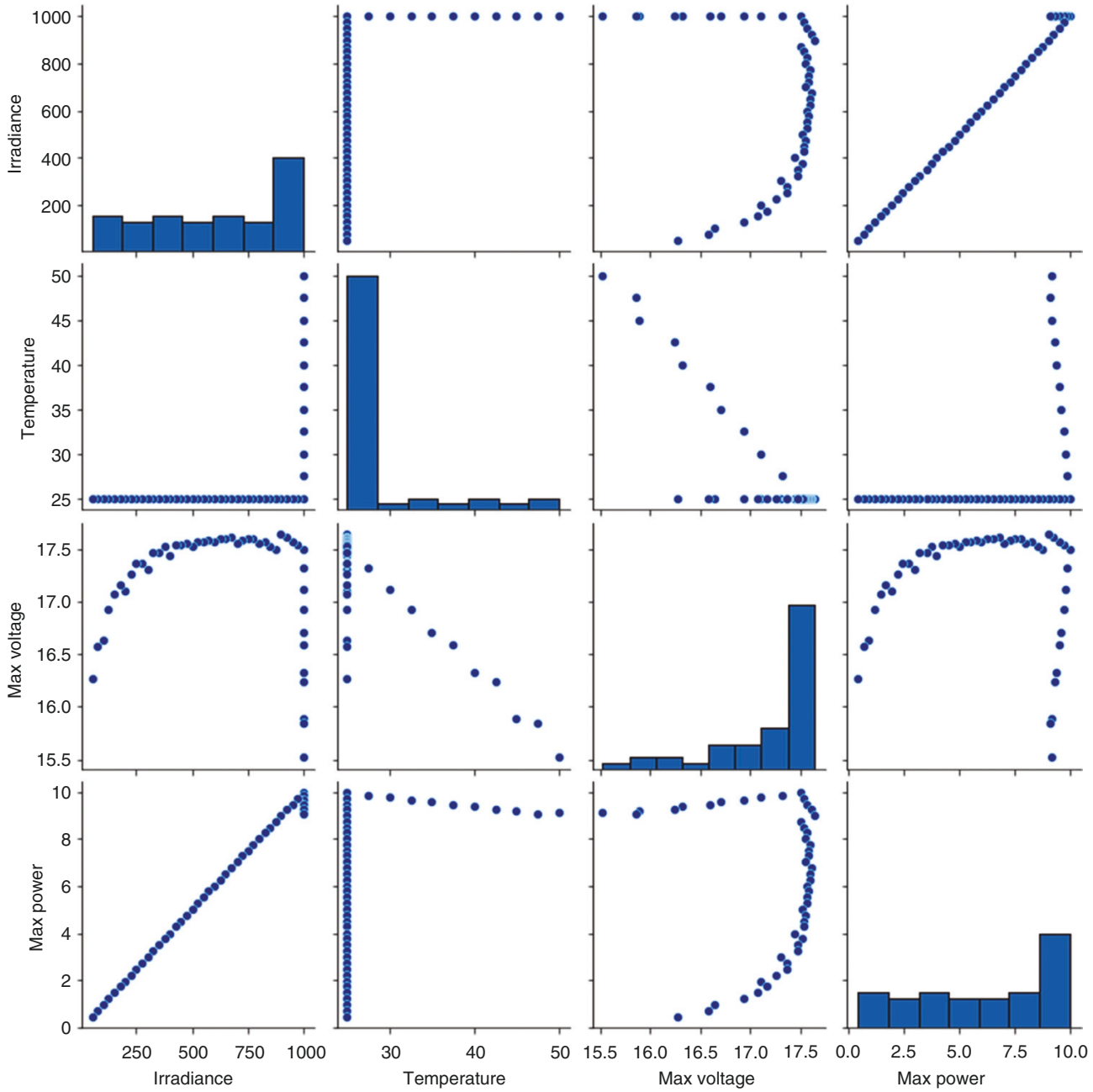

Fig. 10: Pairwise relationship of the variables.

5 Comparative analysis

The developed control strategy's outcomes are compared to those of the β-MPPT method [8], which incorporates the P&O algorithm [5], the CS optimization [12] approach and a perceptron artificial neural network (PANN) algorithm [18, 19].

5.1 β-MPPT method

The fundamental idea behind the β-MPPT approach is to monitor an intermediate variable called β instead of the change in power, which is denoted by Equations (18) and (19):

$$\beta = \ln\left(\frac{i_{pv}}{v_{pv}}\right) - C \times v_{pv} \tag{18}$$

$$C = \frac{q}{NnKT} \tag{19}$$

where i_{pv} and v_{pv}, respectively, stand for the output current and voltage of the PV module. The diode constant is C, q is the electron charge (1.6×10^{-19} coulomb), n is the ideal diode factor and the Boltzmann constant is K, 1.38×10^{-23} J/K, the p–n junction temperature is T in Kelvin and N is the number of PV cells in the module.

This approach's transient and steady-state stages use variable and fixed steps, respectively. Fig. 18 shows the flow chart for this strategy. Before continually calculating the values of β, the current and voltage must first be monitored. The Beta technique enters the steady-state stage if the β is inside the bounding range of the (β_{min}, β_{max}). Otherwise, it enters the temporary stage, in which the P&O method is applied. In the interim stage, the variable step size ΔD is calculated using a guiding parameter β_g, which may be written as Equation (20):

$$\Delta D = F \times (\beta - \beta_g) \tag{20}$$

where F is the scaling factor.

The temperature and irradiance affect the β parameter's range. In this study, β_{min} = 15.45 and β_{max} = 19.02 are used with a scaling factor F = 0.01. The average value of β_{min} and β_{max} was used as β_g = 17.24.

Fig. 19 compares the power response of the β-MPPT (P_{beta}), the maximum power predicted by RT (P_m) and the control technique using the RT algorithm (P_{RT}). For low irradiance levels, the β-MPPT method operates at MPP, but for high irradiance values, this technique fails and exhibits a significant amount of error, preventing the PV system from working at MPP. The system can be operated at MPP in a steady state with more precision using the proposed RT approach compared with the β-MPPT method.

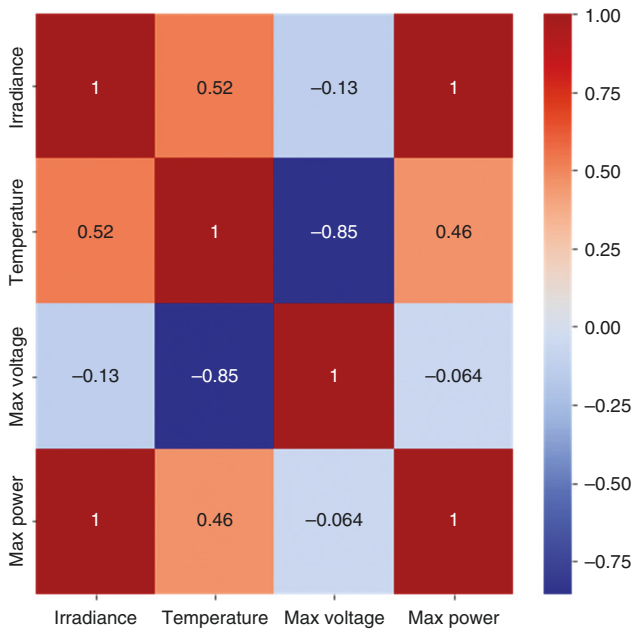

Fig. 11: Heat map of data correlation.

5.2 CS method

The CS method is one of the rapid-converging swarm optimization techniques. The CS approach is implemented as a flow chart in Fig. 20 and creates four new D samples using a series of equations from Equations (21)–(24):

$$D_i^{(t+1)} = D_i^{(t)} + \alpha \oplus \hat{levy}(\lambda); \quad i = 1, 2, 3, 4. \tag{21}$$

where $\alpha = \alpha_o(D_{best} - D_i)$.

Equation (22) gives the simplified Levy flight distribution function [12]:

$$\alpha_o(D_{best} - D_i) \oplus \hat{levy}(\lambda) \approx k_1 \times \left(\frac{u}{|v|^{1/\beta}}\right)(D_{best} - D_i) \tag{22}$$

where β = 1.5 and k_1 (the Levy multiplication coefficient) are equal to 0.8. The normal distribution curve yields the values of u and v, which can be expressed as Equation (23):

$$u \approx N\left(0, \sigma_u^2\right), \quad v \approx N\left(0, \sigma_v^2\right) \tag{23}$$

The σ_u and σ_v values are in Equation (24) with the symbol Γ as integral gamma function:

$$\sigma_v = 1, \ \sigma_u = \left(\frac{\Gamma\ (1+\beta) \times \sin(\pi \times \beta/2)}{\Gamma\ ((1+\beta)/2) \times \beta \times 2^{((\beta-1)/2)}}\right) \tag{24}$$

Fig. 21 compares the P_m predicted by the RT model, the CS method (P_{cs}) and the P_{RT}. The CS method has dynamic behaviour. Initially, the CS response has an undershot, which is undesirable. For small irradiance values, the CS gives good results in tracking MPP. For high irradiance levels, such as 800 W/m^2, the CS technique overshoots and fails to operate the system on MPP, leading to a severe steady-state error. Compared with the CS approach, the

Table 3: Predicted values by RT models, D and percentage mean efficiency for all intervals

Time (sec)	I_r (W/m^2)	T (°C)	P_m (W)	V_m (V)	D	% mean efficiency
0 to 0.5	400	25	3.7612	17.475	0.4798	94.23
0.5 to 1	400	35	3.7612	16.160	0.5189	96.20
1 to 1.5	800	35	7.5258	16.160	0.6599	96.39
1.5 to 2	800	25	7.5258	17.560	0.6304	93.93

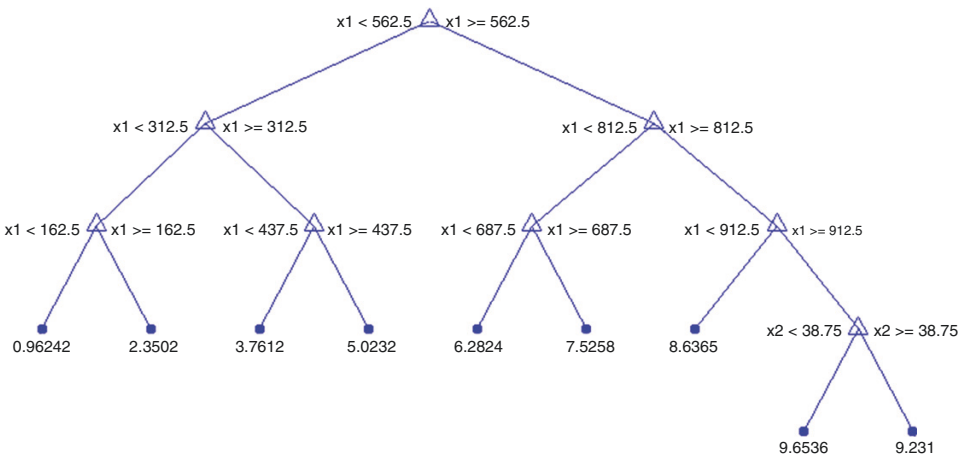

Fig. 12: Developed RT-1 model on the P_m plane.

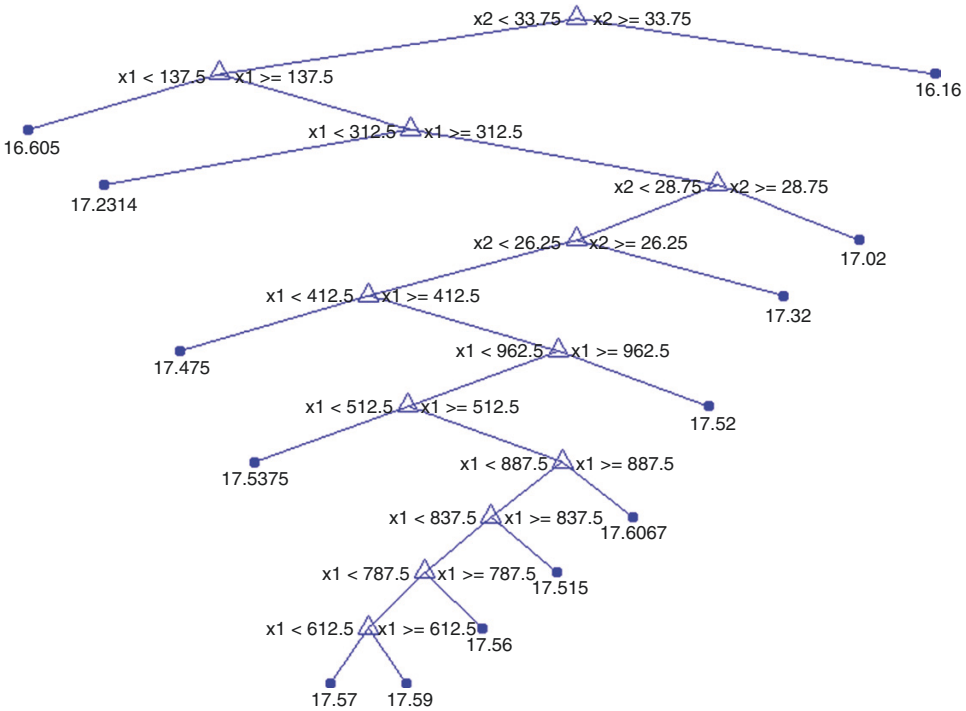

Fig. 13: Developed RT-2 model on the V_m plane.

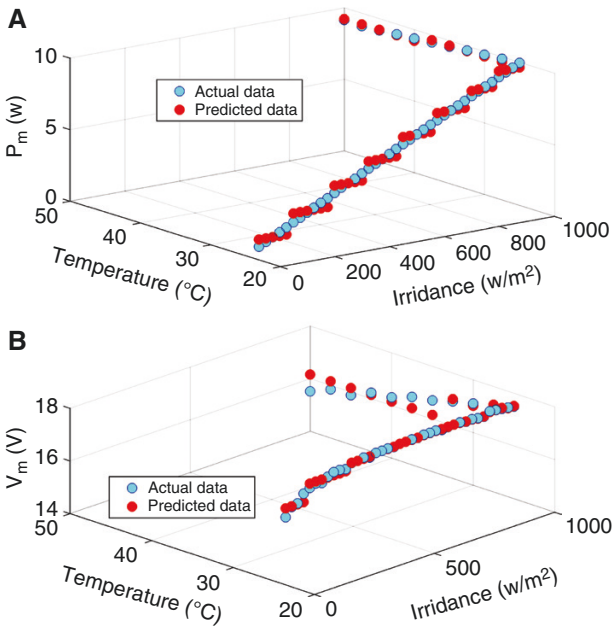

Fig. 14: Actual vs predicted data.(a) RT-1 model on the P_m plane; (b) RT-2 model on the V_m plane.

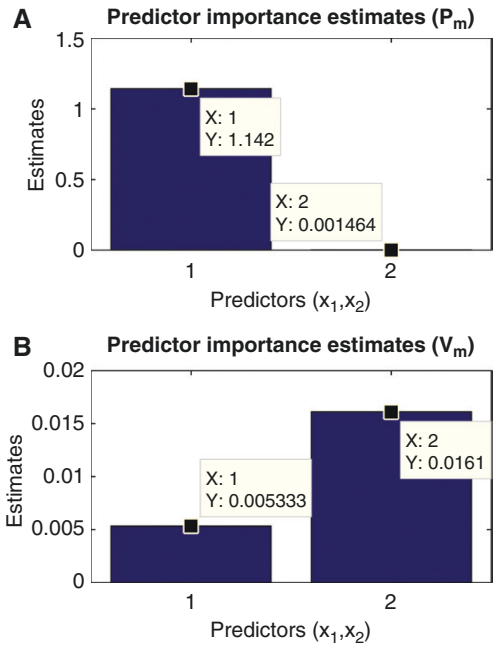

Fig. 15: Predictor importance estimates for (a) RT-1 and (b) RT-2.

proposed RT method produces improved results under varying irradiances and temperatures.

5.3 PANN method

A PANN model with I_r and T as inputs and P_m and V_m as outputs is shown in Fig. 22. A hidden layer having 10 neurons and the output layer with 2 neurons create the constructed PANN model architecture shown in Fig. 22. It has two inputs and two outputs, and all of these layers are interconnected; 60% of the data set was used for training, 20% for validating and the rest for testing the PANN model. The *tansig* and *purelin* activation functions are employed in the hidden and output layers. This linear and non-linear combination of activities produces specific training for the PANN. The role of *tansig* is given as Equation (25) and the delta principle [34] to update the weights ($W_{i,j}$) is shown in Equation (26). The function of *purelin* is in Equation (27) and to update the weights ($W_{j,o}$), the delta principle [34] is in Equation (28):

$$\phi(v_j) = \frac{2}{1+e^{-2v_j}} - 1 \tag{25}$$

$$W_{i,j} \leftarrow W_{i,j} + l_r\, \phi'(v_j)\, e_j x_i \tag{26}$$

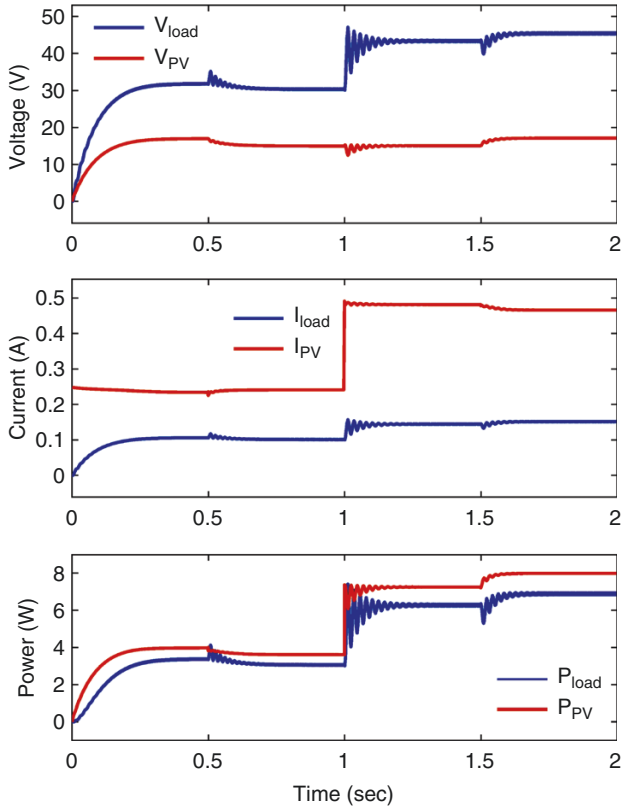

Fig. 16: *V*, *I* and *P* waveforms of the solar panel and load with RT models.

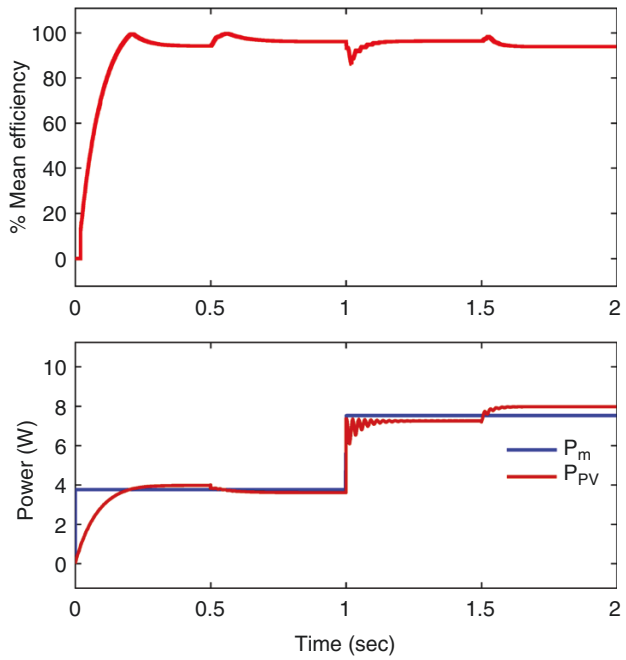

Fig. 17: Percentage mean efficiency, P_m and P_{pv} waveforms with RT models.

where x_i is the present value at the i^{th} (i = 1, 2) input node, $W_{i,j}$ stands for the weight value between the i^{th} input node and the j^{th} hidden node, the learning rate l_r ranges from 0 to 1, the error value at the j^{th} hidden node is e_j, v_j stands for the sum of the weighted inputs including the bias b_j and the derivative value of the *tansig* function is $\phi'(v_j)$:

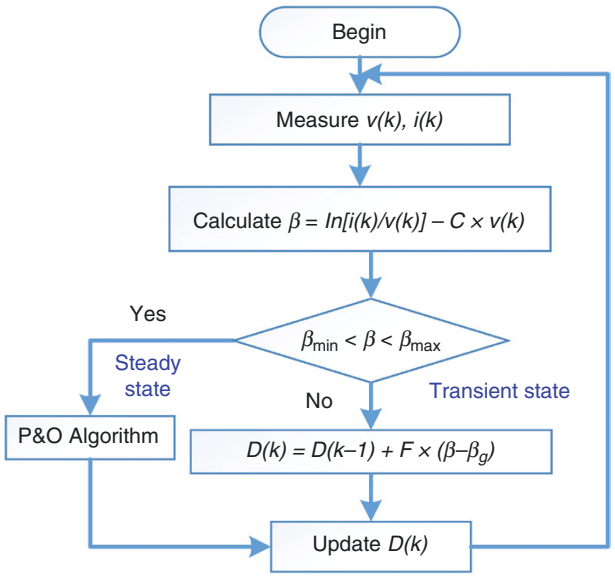

Fig. 18: Flowchart of the Beta MPPT method.

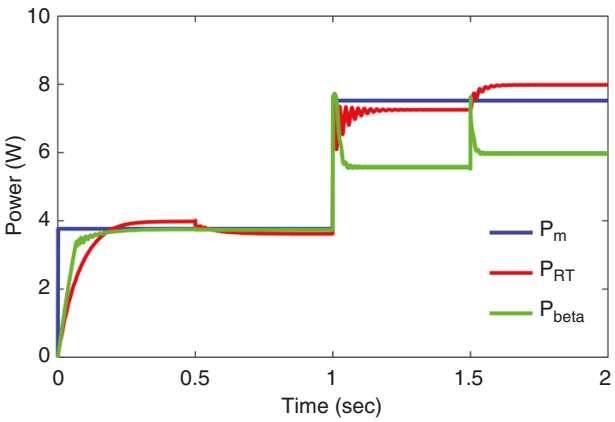

Fig. 19: Power response comparison of P_m, P_{RT} and P_{beta}.

$$\varphi(v_o) = v_o \tag{27}$$

$$W_{j,o} \leftarrow W_{j,o} + l_r\, \varphi'(v_o)\, e_o y_i \tag{28}$$

where the present value of the hidden node *j*, (j = 1, 2,…, 10) is y_j, the weight value between the o^{th} output node and the j^{th} hidden node is $W_{j,o}$, the error value at the output node *o* is e_o, the weighted sum of the hidden nodes together with the bias b_o value is v_o and the derivative value of the *purelin* function is $\varphi'(v_j)$.

To train, validate and test the model, the Levenberg–Marquardt optimization method was used with the same data set used for the proposed methodology. Equation (29) contains the weight-updating formula for determining updated weights ($W_{i,j}^*$ and $W_{j,o}^*$). P_m and V_m were predicted using this PANN model. The train, validate and test regression curves in Fig. 23 demonstrate that R^2 is ~1:

$$\left.\begin{aligned} W_{i,j}^* &= W_{i,j} - [J^TJ - l_pI]^{-1}(J^Te) \\ W_{j,o}^* &= W_{j,o} - [J^TJ - l_pI]^{-1}(J^Te) \end{aligned}\right\} \tag{29}$$

where *J* is the Jacobian matrix, *I* is the identity matrix, *e* is the cumulative error vector and l_p is the learning parameter.

The P_m predicted by the RT model, PANN method (P_{NN}) and P_{RT} is compared in Fig. 24. For low irradiance levels, the PANN response is almost the same as that of the proposed method in this work.

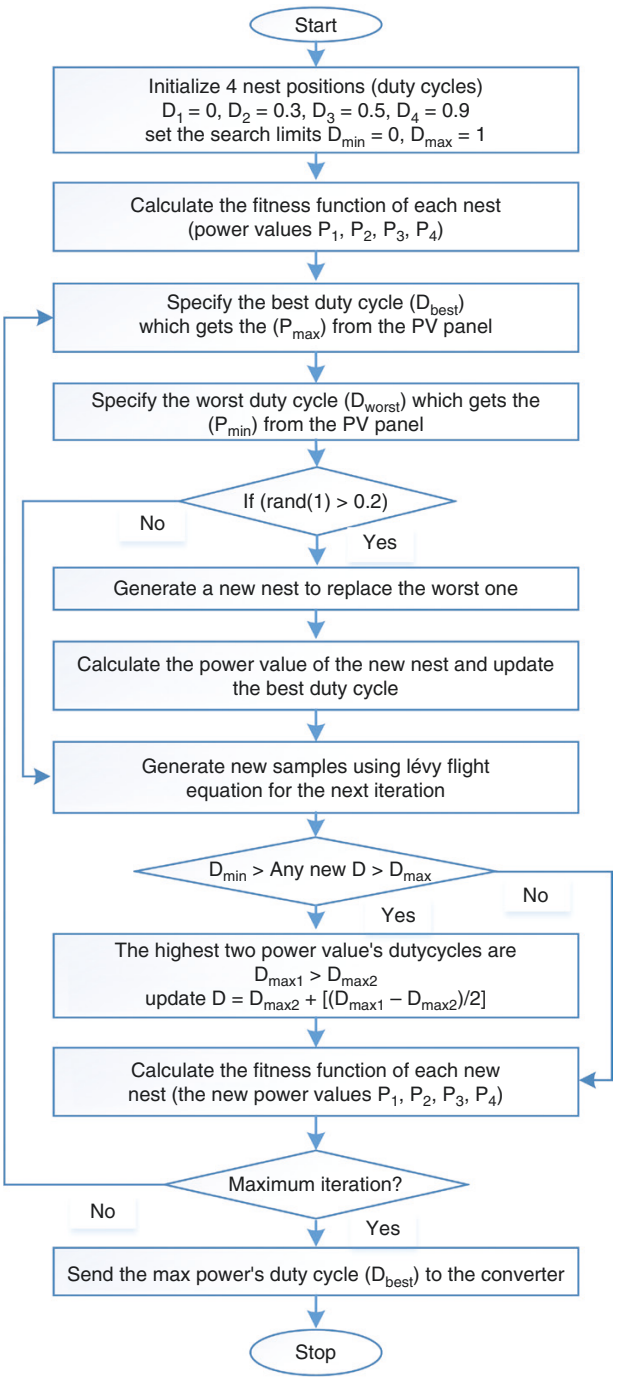

Fig. 20: Flow chart of the CS algorithm.

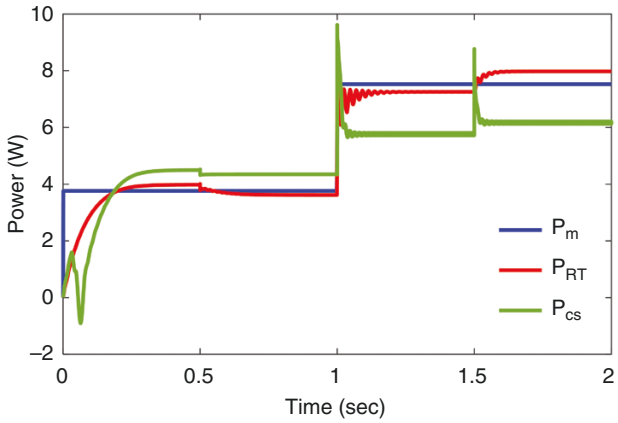

Fig. 21: Power response comparison of P_m, P_{RT} and P_{cs}.

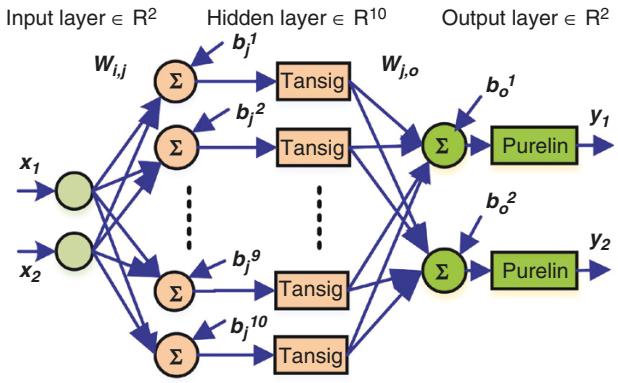

Fig. 22: Architecture of a perceptron neural network with 10 hidden layer neurons.

However, if there is a sudden and colossal rise in irradiance, the PANN response overshoots as shown in the zoomed portion of Fig. 24. If the temperature is decreased, i.e. from 1.5 to 2 sec, the PANN response shows some fixed error in steady state, as shown in Fig. 24. Taken together, the proposed method gives a superior response in tracking the MPP compared to the PANN method.

5.4 Response comparison (during 0–0.5 sec) for all methods used in this work

Comparison of the power response of the proposed, RT predicted, β-MPPT, CS and PANN methods during 0–0.5 s (I_r = 400 W/m^2, T = 25°C) is represented graphically in Fig. 25 and numerically in Table 4. The numerical values of the time domain such as rise time (t_r), peak time (t_p), settling time (t_s), peak overshoot (M_p), minimum settling value (M_m) and peak response value of response for all the methods used are compared in Table 4. Although the β-MPPT response has a good rise time and settling value, the final settling value is poor compared to the rest of the methods. Although the CS method response is better in the peak or settling maximum value, the rise time and settling time are poor compared with the other methods. In addition, the CS response has undershot by ~20%, which is undesirable for the system. Finally, the response of the PANN method is almost perfect but a little poor in terms of all time-domain values compared to the proposed RT control strategy.

6 Conclusions

In this work, a boost converter with PWM control is associated with a new ML-based DT technique for MPPT of the solar panel. The simulation results demonstrate that the developed ML-based control strategy gives a tracking efficiency of >93.93% in tracking MPP, with a quick response in 0.16 sec and the system settles in 0.27 sec. The proposed approach is compared with the β-MPPT, CS optimization and artificial neural network methods under varying temperatures and irradiances to demonstrate its efficacy. The CS has an undershoot of ~20%, which is undesirable for a system, taking 0.21 sec to respond and settling in 0.3 sec. The β-MPPT, CS and PANN methods take 0.06, 0.21 and 0.16 sec to respond and 0.22, 0.3 and 0.29 sec to settle, respectively. Taken together, it is evident that the proposed method shows faster and better accuracy in tracking MPP. The work presented in this paper may be

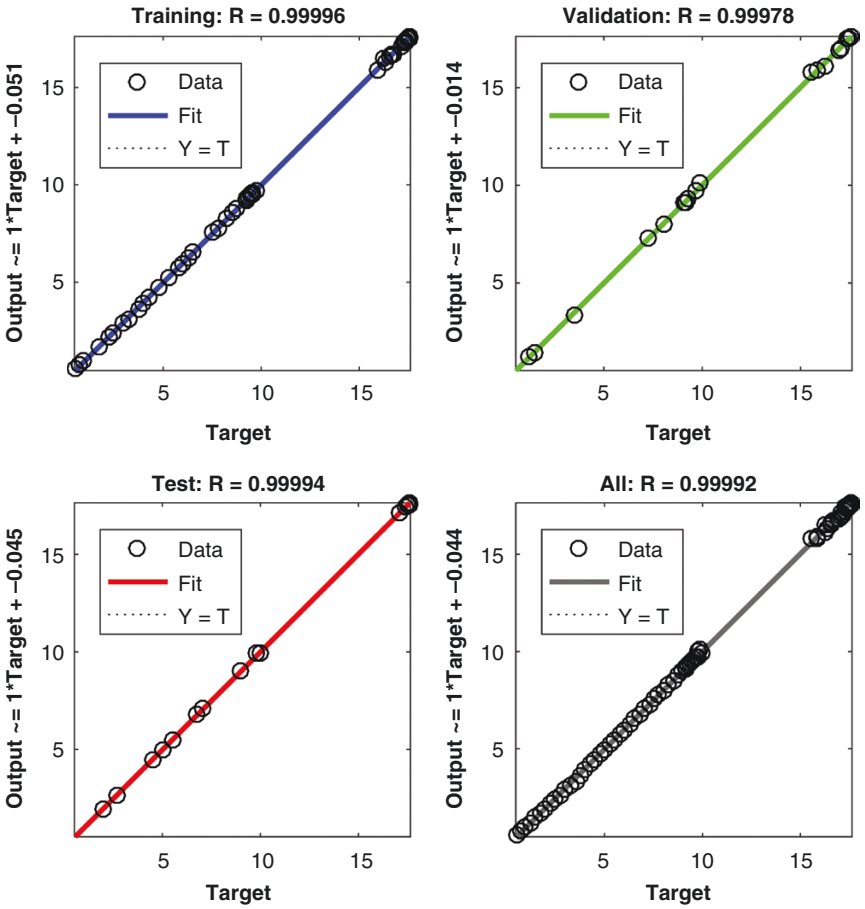

Fig. 23: Training, validation and testing regression plots.

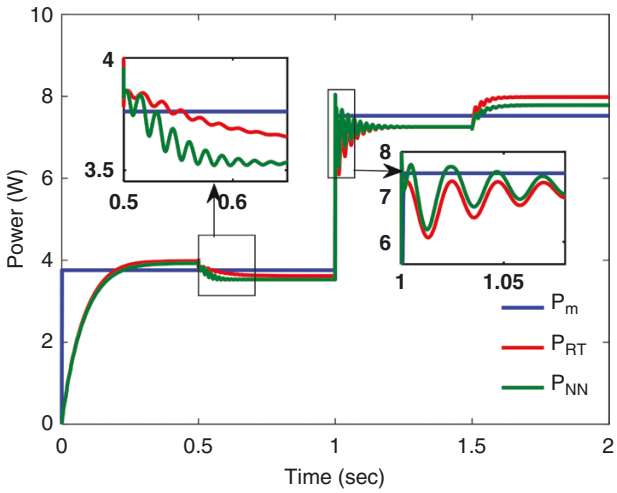

Fig. 24: Comparison of the power response of P_m, P_{RT} and P_{NN}.

Table 4: Comparison of numerical MPP tracking response for different methods during 0–0.5 sec

Parameter	RT	β-MPPT	CS	PANN
t_r (sec)	0.1610	0.0667	0.2114	0.1666
t_p (sec)	0.5	0.5	0.5	0.5
Peak value (W)	4.0081	3.7735	4.5250	3.9532
Min. settling value (W)	3.6073	3.3187	4.0739	3.5579
t_s (sec)	0.2738	0.2185	0.2983	0.2944
Undershoot (%)	0	0	19.9789	0
M_p (%)	0	0	0	0
Energy loss (%)	9.37	8.84	9.86	10.96

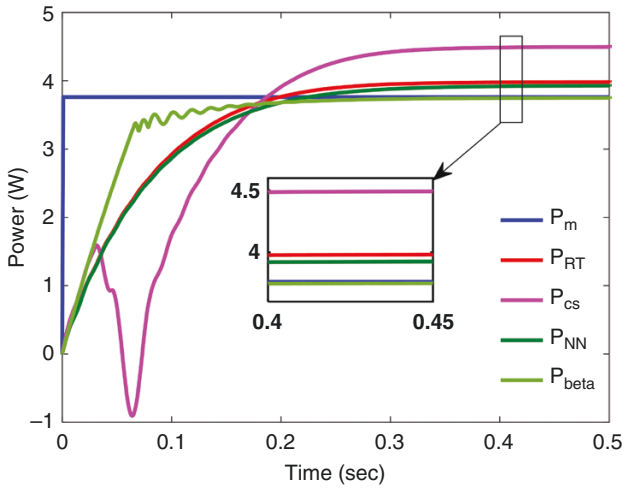

Fig. 25: Comparison of photovoltaic power response for different methods (I_r = 400 W/m^2, T = 25°C).

extended by considering more partial shading effects along with hardware implementation as future scope.

Conflict of interest statement

The authors declare that they have no conflict of interest.

References

[1] *Central Electricity Authority (CEA), India*. https://cea.nic.in/?lang=en (12 September 2022, date last accessed).

[2] Central Electricity Authority (CEA), India. *Annual Report 2020–21*. https://cea.nic.in/wp-content/uploads/annual_reports/2021/CEAAnnualReport_final.pdf (15 August 2022 date last accessed).

[3] Government of India, Ministry of Power. *Power Sector at a Glance all India*. https://powermin.gov.in/en/content/power-sector-glance-all-india (15 August 2022 date last accessed).

[4] Kumar R, Singh SK. Solar photovoltaic modeling and simulation: as a renewable energy solution. *Energy Reports*, 2018, 4:701–712.

[5] Dorji S, Wangchuk D, Choden T, *et al*. Maximum power point tracking of solar photovoltaic cell using perturb & observe and fuzzy logic controller algorithm for boost converter and quadratic boost converter. *Materials Today: Proceedings*, 2020, 27:1224–1229.

[6] Bakar Siddique MA, Asad A, Asif RM, *et al*. Implementation of incremental conductance MPPT algorithm with integral regulator by using boost converter in grid-connected PV array. *IETE Journal of Research*, 2021. doi: 10.1080/03772063.2021.1920481

[7] Shang L, Guo H, Zhu W. An improved MPPT control strategy based on incremental conductance algorithm. *Protection and Control of Modern Power Systems*, 2020, 5:1–8.

[8] Li X, Wen H, Jiang L, *et al*. Photovoltaic modified β-parameter-based MPPT method with fast tracking. *Journal of Power Electronics*, 2016, 16:9–17.

[9] González-Castaño C, Lorente-Leyva LL, Muñoz J, *et al*. An MPPT strategy based on a surface-based polynomial fitting for solar photovoltaic systems using real-time hardware. *Electronics*, 2021, 10:206.

[10] Baimel D, Tapuchi S, Levron Y, *et al*. Improved fractional open circuit voltage MPPT methods for PV systems. *Electronics*, 2019, 8:321.

[11] Başoğlu ME. An approximate short circuit strategy for transient MPPT performance of uniformly irradiated photovoltaic modules. *Balkan Journal of Electrical and Computer Engineering*, 2019, 7:88–93.

[12] Abo-Elyousr FK, Abdelshafy AM, Abdelaziz AY. MPPT-based particle swarm and cuckoo search algorithms for PV systems. In: Eltamaly AM, Abdelaziz AY, (eds). *Modern Maximum Power Point Tracking Techniques for Photovoltaic Energy Systems*. New York: Springer, 2020, 379–400.

[13] Wei L, Li K. Research on the maximum power point tracking method of photovoltaic based on Newton interpolation-assisted particle swarm algorithm. *Clean Energy*, 2022, 6:496–502.

[14] Chao KH, Rizal MN. A hybrid MPPT controller based on the genetic algorithm and ant colony optimization for photovoltaic systems under partially shaded conditions. *Energies*, 2021, 14:29022902.

[15] Hadji S, Gaubert JP, Krim F. Real-time genetic algorithms-based MPPT: study and comparison (theoretical an experimental) with conventional methods. *Energies*, 2018, 11:459.

[16] Zdiri MA, Khelifi B, Salem FB, *et al*. Comparative study of distinct advanced MPPT algorithms for a PV boost converter. *International Journal of Renewable Energy Research*, 2021, 11:1156–1165.

[17] Khelifi B, Salem FB, Zdiri MA, *et al*. Stand-alone PV-PEMFC system based SMANN-MPPT controller: solar pumping application using PMSM. *International Journal of Renewable Energy Research*, 2021, 11:662–672.

[18] Villegas-Mier CG, Rodriguez-Resendiz J, Álvarez-Alvarado JM, *et al*. Artificial neural networks in MPPT algorithms for optimization of photovoltaic power systems: a review. *Micromachines*, 2021, 12:12601260.

[19] Mantri R, Raghavendra KR, Puri H, *et al*. Weather prediction and classification using neural networks and k-nearest neighbors. In: *IEEE International Conference on Smart Computing and Communications (ICSCC)*, Kochi, Kerala, India, 1–3 July 2021, 263–268. doi: 10.1109/ICSCC51209.2021.9528115.

[20] Asif RM, Siddique MAB, Rehman AU, *et al*. Modified fuzzy logic MPPT for PV system under severe climatic profiles. *Pakistan Journal of Engineering and Technology*, 2021, 4:49–55.

[21] Asif RM, Ur Rehman A, Ur Rehman S, *et al*. Design and analysis of robust fuzzy logic maximum power point tracking based isolated photovoltaic energy system. *Engineering Reports*, 2020, 2:e12234.

[22] Li X, Wen H, Hu Y, *et al*. A novel beta parameter based fuzzy-logic controller for photovoltaic MPPT application. *Renewable Energy*, 2019, 130:416–427.

[23] Mahesh PV, Meyyappan S, Alla RKR. A new multivariate linear regression MPPT algorithm for solar PV system with boost converter. *ECTI Transactions on Electrical Engineering, Electronics, and Communications*, 2022, 20:269–281.

[24] Mo S, Ye Q, Jiang K, *et al*. An improved MPPT method for photovoltaic systems based on mayfly optimization algorithm. *Energy Reports*, 2022, 8:141–150.

[25] Revathy SR, Kirubakaran V, Rajeshwaran M, *et al*. Design and analysis of ANFIS–based MPPT method for solar photovoltaic applications. *International Journal of Photoenergy*, 2022, 2022:9625564.

[26] Rafeeq Ahmed K, Sayeed F, Logavani K, *et al*. Maximum power point tracking of PV grids using deep learning. *International Journal of Photoenergy*, 2022, 2022:11123251–11123257.

[27] Islam H, Mekhilef S, Shah NM, *et al*. Improved proportional-integral coordinated MPPT controller with fast tracking speed for grid-tied PV systems under partially shaded conditions. *Sustainability*, 2021, 13:830.

[28] Rajani K, Ramesh T. Maximum power enhancement under partial shadings using a modified Sudoku reconfiguration. *CSEE Journal of Power and Energy Systems*, 2020, 7:1187–1201.
[29] Phan BC, Lai YC, Lin CE. A deep reinforcement learning-based MPPT control for PV systems under partial shading condition. *Sensors*, 2020, 20:3039.
[30] Carballo JA, Bonilla J, Berenguel M, *et al*. Machine learning for solar trackers. *AIP Conference Proceedings*, 2019, 2126:030012.
[31] Shareef H, Mutlag AH, Mohamed A. Random forest-based approach for maximum power point tracking of photovoltaic systems operating under actual environmental conditions. *Computational Intelligence and Neuroscience*, 2017, 2017:1673864.
[32] Ayop R, Tan CW. Design of boost converter based on maximum power point resistance for photovoltaic applications. *Solar Energy*, 2018, 160:322–335.
[33] Rashid MH. *Power Electronics: Circuits, Devices & Applications*. 4th edn. London: Pearson, 2004.
[34] Kim P. *MATLAB Deep Learning With Machine Learning, Neural Networks and Artificial Intelligence*. 1st edn. Berkeley, CA: Apress, 2017.